



## Silicide formation on a Pt/SiO<sub>2</sub> model catalyst studied by TEM, EELS and EDXS

D. Wang<sup>a,\*</sup>, S. Penner<sup>b</sup>, D. S. Su<sup>a</sup>, G. Rupprechter<sup>c</sup>, K. Hayek<sup>b</sup>, R. Schlögl<sup>a</sup>

<sup>a</sup>Department of Inorganic Chemistry, Fritz-Haber-Institute of the MPG, Faradayweg 4-6, 14195 Berlin, Germany

<sup>b</sup>Institut für Physikalische Chemie, Leopold-Franzens-Universität, A-6020 Innsbruck, Austria

<sup>c</sup>Department of Chemical Physics, Fritz Haber Institute of the Max Planck Society, Faradayweg 4-6, 14195 Berlin, Germany

Received 10 March 2003; accepted 05 May 2003

\* Corresponding author: e-mail [wangdi@fhi-berlin.mpg.de](mailto:wangdi@fhi-berlin.mpg.de), phone +49 30 8413 4482, fax +49 30 8413 4401

### Abstract

Dispersed Pt particles supported by amorphous SiO<sub>2</sub> were grown with regular shapes and orientation along the same crystallographic axis ("initial state"). After an oxidising treatment the samples were heated in 1 bar hydrogen at 873 K. The morphological and structural changes were studied by transmission electron microscopy (TEM). Platinum silicide Pt<sub>3</sub>Si with L1<sub>2</sub> (Cu<sub>3</sub>Au) structure, monoclinic Pt<sub>3</sub>Si and tetragonal Pt<sub>12</sub>Si<sub>5</sub> were identified after the treatment. A topotactic structural transformation accompanied by the migration of Si from the substrate to the particles is suggested to take place during Pt<sub>3</sub>Si formation. Pt<sub>12</sub>Si<sub>5</sub> is formed through melting and recrystallisation. The mechanisms of reconstruction of the crystallites are discussed.

**Keywords:** Platinum silicide; Metal support interaction; Catalysis; Electron diffraction; High-resolution electron microscopy; Electron energy-loss spectroscopy

### Introduction

Dispersed metal particles supported on porous substrates are widely applied in heterogeneous catalysis. The catalysts usually show activities and selectivities strongly depending on the pretreatment (cleaning/activation) conditions. The noble metal may interact with both reducible (*e.g.* TiO<sub>2</sub>) and non-reducible (*e.g.* SiO<sub>2</sub> and Al<sub>2</sub>O<sub>3</sub>) oxide supports [1–3]. This metal support interaction may have drastic effects on the chemisorptive and catalytic properties of the metal phase. Therefore, the investigation of the changes under various treatment conditions, regarding surface and internal structure, morphology, and electronic structure, is of great importance for elucidating the mechanism of the metal support interaction and the correlation between structure and catalytic properties.

In view of the complexity of "real" supported catalysts, consisting of randomly oriented and irregularly shaped metal particles on high surface area porous supports, well oriented

and regularly shaped metal particles grown on planar thin supports are frequently used as model catalysts. This facilitates the study of the structure, the electronic properties and the catalytic activation of the catalysts by surface science and TEM techniques [4–6]. In our previous studies [7], small particles of noble metals like Pt, Rh, Ir, or Pd were grown by means of high vacuum deposition on NaCl cleavage faces or on in-situ deposited NaCl films at 523–673 K. The particles were covered with a supporting film of Al<sub>2</sub>O<sub>3</sub> or carbon and the film was then removed from the substrate. Rh/Al<sub>2</sub>O<sub>3</sub> and Pt/Al<sub>2</sub>O<sub>3</sub> films prepared in such a way were subjected to oxidising and reducing atmospheres. Their TEM characterization shows high-index facets formed after oxidation between 523 and 773 K and low-index facets restored after reduction in hydrogen around 723 K [6, 8]. Pt or Rh particles grown in pure hydrogen on planar SiO<sub>2</sub> or Al<sub>2</sub>O<sub>3</sub> flakes show a similar behaviour upon oxidation and reduction. These results were explained by the approach to a hydrogen-induced equilibrium shape [9, 10].

After a reduction at higher temperature, metal support interaction with the formation of intermetallic compounds was observed in various metal-oxide systems. NiSi<sub>3</sub> with Cu<sub>3</sub>Au structure was revealed by TEM after heating Ni/SiO<sub>2</sub> at 850 K in hydrogen [11]. Reduction of Pd/SiO<sub>2</sub> in hydrogen at 845 K led to the growth of PdSi<sub>2</sub> and the pretreatment of the support strongly influenced the metal support interaction [12]. Recently, X-ray diffraction studies on Pd/SiO<sub>2</sub> suggested a stepwise phase change from Pd<sub>4</sub>Si to Pd<sub>3</sub>Si during the reduction in hydrogen at 873 K [13]. Changes in dispersion and chemical composition were reported for Pt/SiO<sub>2</sub> heated in hydrogen at 773 K and 823 K and the new phase formed at 823 K was attributed to Pt<sub>2</sub>Si and Pt<sub>3</sub>Si [14]. After heating a similar Pt/SiO<sub>2</sub> system at 840 K in hydrogen, a Pt<sub>3</sub>Si phase with cubic Cu<sub>3</sub>Au structure was identified as an intermediate to monoclinic Pt<sub>3</sub>Si, which appeared after additional heating at 1020 K in hydrogen [15]. Platinum silicide formation on a Pt-SiO<sub>2</sub> model catalyst fabricated by electron beam lithography (EBL) was also reported by Zhu and Somorjai [16]. However, in this case the silicide formation was induced by sputtering with Ne ions during sample cleaning. The sputtering process presumably facilitated the silicide formation by intermixing Pt and Si atoms. When Rupprechter et al. [17, 18] subjected the same EBL samples to annealing treatments in vacuum up to 1173 K the Pt particles formed larger crystalline domains (intraparticle recrystallization) but no silicides were observed.

Among all the Pt silicides, the cubic Pt<sub>3</sub>Si was reported to have an L1<sub>2</sub> (Cu<sub>3</sub>Au) structure with space group  $Pm\bar{3}m$ , and its lattice parameter,  $a = 3.88 \text{ \AA}$ , is decreased by only 1% with respect to that of Pt,  $a_0 = 3.92 \text{ \AA}$ . The monoclinic Pt<sub>3</sub>Si phase has space group C2/m and the lattice parameters  $a = 7.702 \text{ \AA}$ ,  $b = c = 7.765 \text{ \AA}$  and  $\beta = 88^\circ 11'$  [19]. It can be regarded as a distorted Cu<sub>3</sub>Au structure. Pt<sub>12</sub>Si<sub>5</sub> and Pt<sub>2</sub>Si do not show an obvious structural relationship with Pt<sub>3</sub>Si or Pt. The space group of Pt<sub>12</sub>Si<sub>5</sub> is P4/n with lattice parameters  $a = b = 13.404 \text{ \AA}$  and  $c = 5.451 \text{ \AA}$  [20]. The space group of Pt<sub>2</sub>Si is I4/mmm with lattice parameters  $a = b = 3.933 \text{ \AA}$  and  $c = 5.91 \text{ \AA}$  [19]. The structure models of cubic Pt<sub>3</sub>Si, monoclinic Pt<sub>3</sub>Si, Pt<sub>12</sub>Si<sub>5</sub> and Pt<sub>2</sub>Si are shown in Figs. 1a–d.

In our previous studies on systems of Pt/SiO<sub>2</sub>, Pt/Al<sub>2</sub>O<sub>3</sub> and Pt/CeO<sub>2</sub>, several Pt silicides were distinguished [21]. However, only limited fine structural information of individual particles was obtained. In the present work, the morphology of regular silica-supported Pt particles and their interaction with the support during the treatment in hydrogen at 873 K were intensively investigated by TEM, electron energy-loss spectroscopy (EELS) and energy-dispersive X-ray spectroscopy (EDXS). Mechanisms of intermetallic compound formation and of crystallite reconstruction are proposed.

## Experimental

Pt particles were grown at 623 K by electron beam evaporation of Pt at a pressure of 10<sup>-6</sup> mbar on vacuum-cleaved (001) NaCl single crystals. They were covered with a thin supporting film of amorphous silica (25 nm thick), prepared by reactive deposition of SiO in 10<sup>-4</sup> mbar oxygen. Subse-

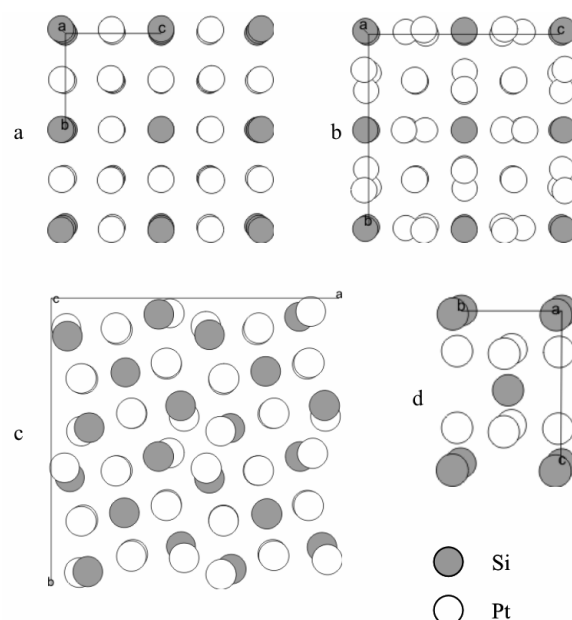


**Fig. 1.** The structure models of (a) cubic Pt<sub>3</sub>Si on [100] projection, (b) monoclinic Pt<sub>3</sub>Si on [100] projection, (c) Pt<sub>12</sub>Si<sub>5</sub> on [001] projection and (d) Pt<sub>2</sub>Si on [100] projection.

quently, the NaCl was dissolved in distilled water and the films were washed and mounted on gold grids. After an oxidising treatment in O<sub>2</sub> at 673 K for 1 h, the reduction was performed with 1 bar hydrogen gas at 873 K for 1 h. The morphology and structure of the samples were then examined ex-situ in a Philips CM200 FEG microscope using selected area electron diffraction (SAED), bright field imaging, microdiffraction, high-resolution imaging, EELS and EDXS.

## Results

Both the as-grown sample and that after the treatment were

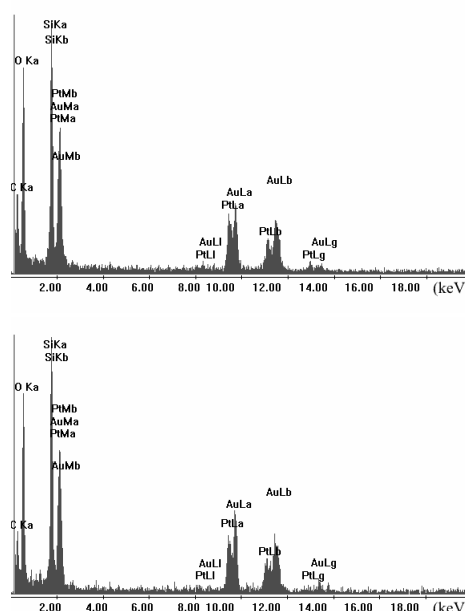


**Fig. 2.** EDX spectra from (a) the as-grown sample and (b) the sample after the treatment.

examined by EDXS. Si, O, Pt and Au signals from the grid, as well as a small amount of C were detectable (cf. Fig. 2). The weak C signals could be due to C deposition during the TEM observation.

### Low-magnification images

Fig. 3a shows the low-magnification image of the as-grown

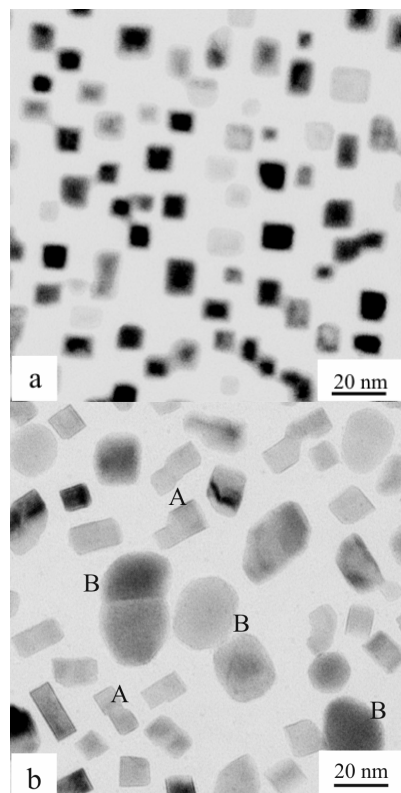


**Fig. 3.** Low-magnification image of silica supported Pt particles (a) before and (b) after the reduction in H<sub>2</sub> at 873 K.

Pt particles. Most of them exhibit square or rectangular shapes with edges parallel to each other. These particles were identified as (truncated) half octahedra by weak-beam dark field imaging [7]. The size of the particles amounts to 8–15 nm. Subsequent oxidation (1 bar O<sub>2</sub>, 673K, 1h) does not lead to significant changes, except for the appearance of higher-indexed facets [7]. The electron micrograph of the particles after a reductive treatment at 873K in hydrogen reveals a significant change in the morphology. Particles consisting of two rectangular parts (denoted as A in Fig. 3b) and large particles with irregular forms (denoted as B in Fig. 3b) were observed. These particles are about 20 nm in size. In addition, a number of particles exhibit a characteristic platelet shape with sharp edges. Obviously, the particles after the treatment are more randomly oriented than the as-grown ones.

### Electron diffraction

The SAED patterns of the samples before and after the treatment are shown in Figs. 4a and 4b, respectively, which

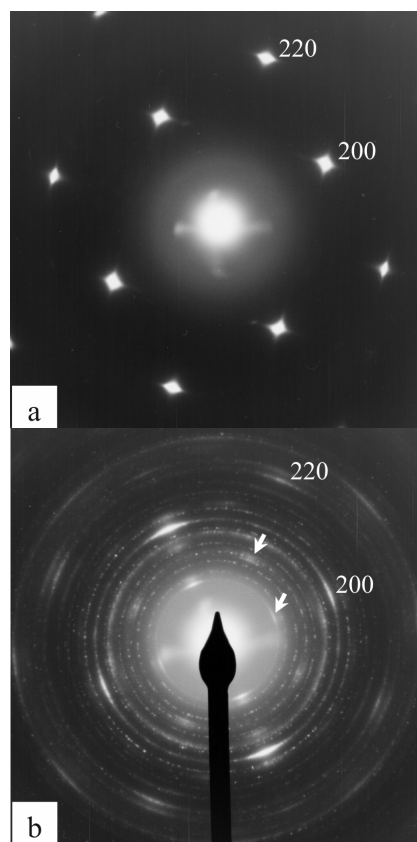


**Fig. 4.** Electron diffraction patterns of silica supported Pt particles (a) before and (b) after the reduction in H<sub>2</sub> at 873 K.

give further information about the structure modification. The pattern in Fig. 4a is identical to the pattern of a [001]-oriented Pt single crystal, i.e., all the as-grown particles exhibit the same orientation, which is due to their epitaxial growth on the (001) NaCl surface. In contrast, the diffraction pattern of the sample after the treatment shows a series of rings together with some diffuse, but distinct spots.

Calibrated by the electron diffraction pattern of Pt before the treatment, the interplanar distances  $d$  ( $\pm 1\%$ ) are calculated from rings and diffuse spots in Fig. 4b and are listed in Table 1. The diffraction intensities corresponding to the positions of the Pt 200 and 220 reflections can still be distinguished upon a series of rings. Additional spots are found corresponding to the positions of the 100 and 110 reflections (denoted in Fig. 4b by arrows), which are forbidden diffractions for the face-centered cubic structure. Comparing the  $d$  values of all the rings and diffuse spots with those of the reported Pt silicide, which are also shown in Table 1, we found that the new phase formation can be attributed to cubic Pt<sub>3</sub>Si, monoclinic Pt<sub>3</sub>Si, and tetragonal Pt<sub>12</sub>Si<sub>5</sub>. The appearance of the seemingly forbidden diffractions corresponding to Pt 100 and 110 diffractions probably arises from 100 and 110 diffractions of cubic Pt<sub>3</sub>Si or 200, 020, 002, 220, 022 and 202 diffractions of monoclinic Pt<sub>3</sub>Si. These newly appeared diffractions show relatively strong intensities and coincide with Pt 200 and 220 diffractions in azimuth orientation. This indicates that in a considerable

**Table 1** Measured interplanar distances *d* compared with those of Pt<sub>3</sub>Si (cubic) Pt<sub>3</sub>Si (monoclinic), Pt<sub>12</sub>Si<sub>5</sub> and Pt

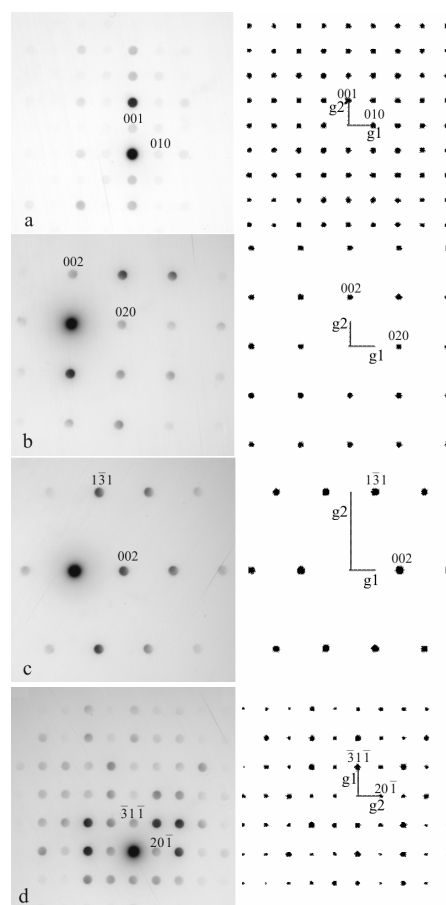
<i>d</i> (Å)	Pt <sub>3</sub> Si (cubic)		Pt <sub>3</sub> Si (monoclinic)		Pt <sub>12</sub> Si <sub>5</sub> (tetragonal)		Pt	
	<i>d</i> (Å)	( <i>hkl</i> )	<i>d</i> (Å)	( <i>hkl</i> )	<i>d</i> (Å)	( <i>hkl</i> )	<i>d</i> (Å)	( <i>hkl</i> )
3.91	3.88	(100)	3.88	(002)				
3.45					3.48	(301)		
3.00					3.01	(420)		
2.76	2.75	(110)	2.78	(202)	2.76	(331)		
2.69			2.69	( $\bar{2}02$ )				
2.46								
2.36			2.36	(113)	2.36	(222)		
2.20			2.21	( $\bar{2}22$ )				
2.13					2.13	(620)		
1.96	1.94	(200)					1.96	(200)
1.81			1.80	(313)	1.82	(003)		
1.50			1.50	(115)				
1.38	1.37	(220)	1.39	(404)			1.39	(220)
1.31								
1.18	1.17	(311)					1.18	(311)

number of particles Pt<sub>3</sub>Si is formed topotactically with the original Pt [001] zone and azimuth orientation preserved. Most of the other rings in Fig. 4b can be attributed to monoclinic Pt<sub>3</sub>Si and Pt<sub>12</sub>Si<sub>5</sub>.

In addition, microdiffraction patterns are taken from individual particles after the reduction treatment and are shown in Figs. 5a–d. Simulated diffraction patterns are calculated using the EMS online package [22] to verify the structure determination (at the right side of each experimental diffraction pattern). Most particles with platelet shape and straight edges produce similar microdiffraction patterns, one of which is shown in Fig. 5a. It is indexed as Cu<sub>3</sub>Au type Pt<sub>3</sub>Si on a [100] zone axis. Figs. 5b and 5c show the diffraction patterns from Pt on [100] and [310] zone axes, respectively. This confirms the existence of not reacted Pt after the reduction treatment. For some of them the base plane and azimuth orientation have changed. Particles with irregular forms usually show various diffractions and a considerable amount of them can be attributed to Pt<sub>12</sub>Si<sub>5</sub>. One such microdiffraction pattern is shown in Fig. 5d, which exhibits a [152] zone axis of Pt<sub>12</sub>Si<sub>5</sub>. The simulated diffraction patterns are in agreement with the experimental ones indicating the validity of the indexing.

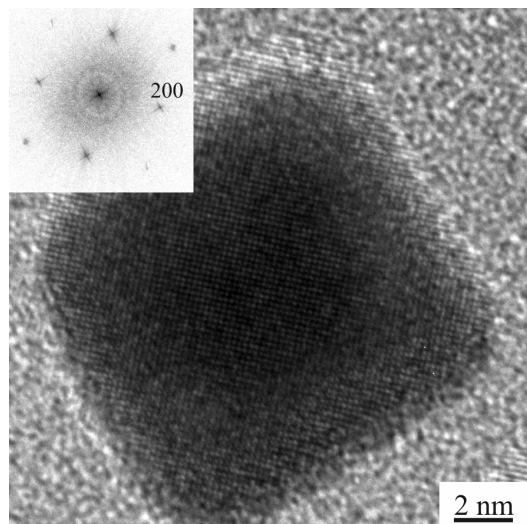
### High-resolution imaging

High-resolution images are taken from various particles with different sizes and shapes before and after the reduction. With Fourier transform analysis to the high-resolution images, comprehensive structural information regarding the particle coalescence and the phase overlapping is obtained in addition to the phase identification.



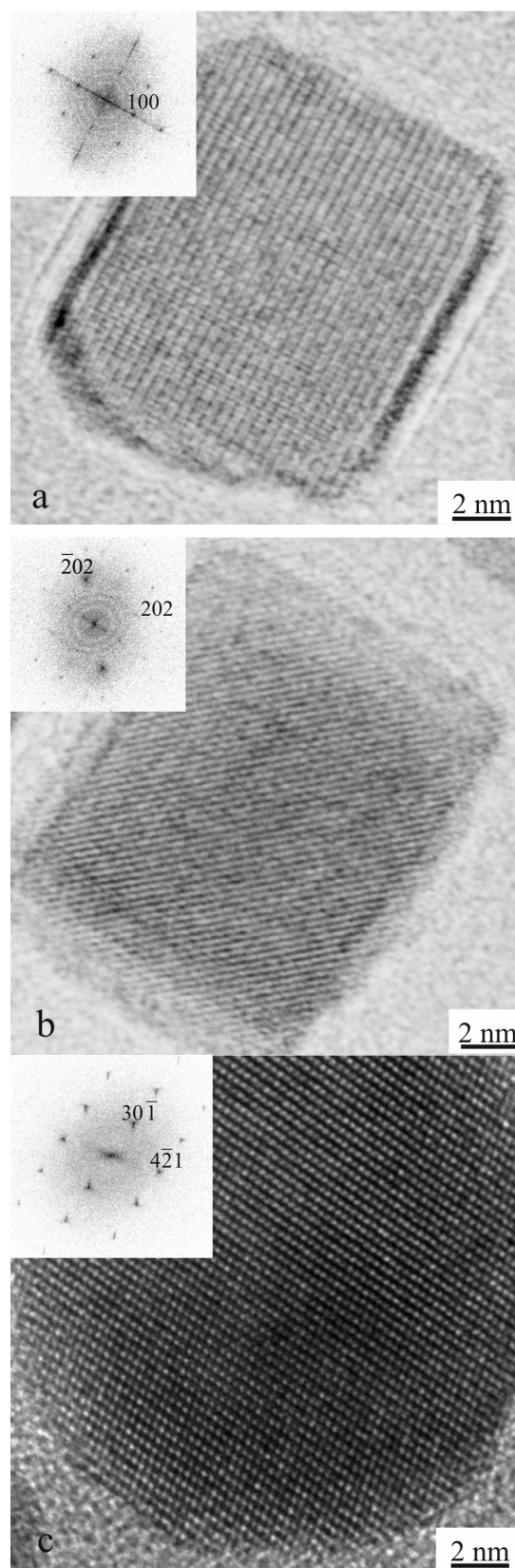
**Fig. 5.** Microdiffraction patterns from four single particles after the reduction, indexed as (a) [100] Pt<sub>3</sub>Si, (b) [100] Pt, (c) [310] Pt and (d) [152] Pt<sub>12</sub>Si<sub>5</sub>.

Fig. 6 shows the high-resolution image of one as-grown Pt particle with its Fourier transform inset. The lattice fringes in Fig. 6 have an interval of 1.96 Å corresponding to the 200 reflection of Pt in the Fourier transform. The (200) planes are rotated by 45° with respect to the particle edges lying along the [220] direction.



**Fig. 6.** High-resolution image of an as-grown Pt particle, with its Fourier transform inset.

The high-resolution images of the particles after the reduction treatment at 873 K clearly show the structural change due to the formation of intermetallic compounds. Three particles with even contrast are shown in Figs. 7a–c. The lattice fringe interval in Fig. 7a is about 3.9 Å, which can be attributed to cubic Pt<sub>3</sub>Si. Accordingly, the "100" reflections appear in its Fourier transform. The Fourier transform in Fig. 7b is quite similar to that in Fig. 7a. However, a careful analysis shows that the primary vectors are not perpendicular to each other. The angle between them is measured as about 88°, which cannot be simply explained as a measurement error. The two reflections in the Fourier transform are indexed as  $\bar{2}02$  and 202, respectively, because the vector lengths of these two reflections differ from each other by a small amount, which coincides well with the parameters of monoclinic Pt<sub>3</sub>Si having  $d_{\bar{2}02} = 2.69$  Å and  $d_{202} = 2.76$  Å. Therefore, the structure in Fig. 7b is determined as monoclinic Pt<sub>3</sub>Si and the image was taken near the [010] zone axis. Figs. 7a and 7b are representative of most particles with rectangular platelet shape and sharp parallel edges. For these particles, however, the (100) planes of cubic Pt<sub>3</sub>Si, as well as the (200), (020), or (002) planes of monoclinic Pt<sub>3</sub>Si are all parallel to the particle edges, different from the as-grown Pt particles exhibiting 45° between the (200) plane and the particle edge. In agreement with the results of microdiffraction, Pt<sub>12</sub>Si<sub>5</sub> is mainly found in particles with round shape and shows various zone axes. This points to the formation of Pt<sub>12</sub>Si<sub>5</sub> by melting and recrystallisation. Fig. 7c shows the high-resolution image of one such



**Fig. 7.** High-resolution images of three particles after the reduction revealing the formation of new phases of (a) Pt<sub>3</sub>Si with L12 structure, (b) monoclinic Pt<sub>3</sub>Si and (c) Pt<sub>12</sub>Si<sub>5</sub>. The corresponding Fourier transforms are inserted.

particle. The Fourier transform analysis indicates that the projected structure can be attributed to Pt<sub>12</sub>Si<sub>5</sub> on its [276]

zone axis. Reflections of  $30\bar{1}$  and  $4\bar{2}1$  are indicated in the Fourier transform.

After the reduction at 873 K, a considerable amount of particles also show coalescence of two or more crystallites. Fig. 8a shows the beginning stages of a coalescence process of

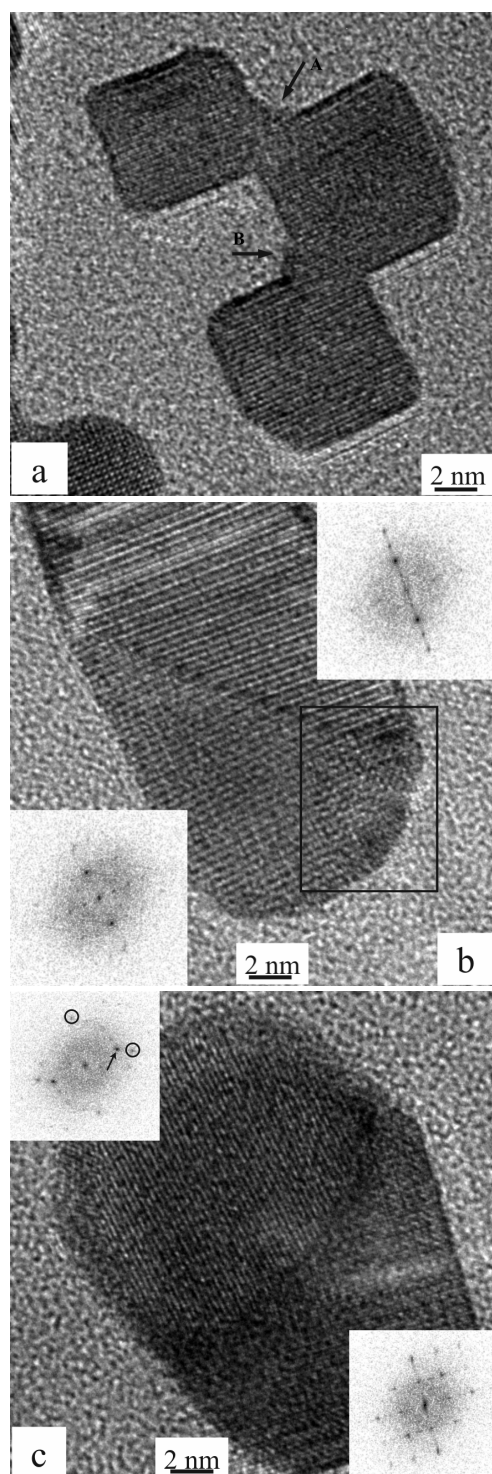


**Fig. 8.** High-resolution images of particles after the reduction, showing (a) the coalescence of three particles, (b) the coalescence of two crystallites with an interface formed in between and (c) the overlapping of different phases.

three particles with platelet shape. It can be seen that each two particles coagulate at the corners. A detailed study of the micrograph reveals that the contacting area exhibits curved edges and shows either a contrast differing from those of the particles (arrowed A) or lattice fringes showing a grain boundary (arrowed B). The difference in contrast and the existence of a grain boundary indicate the rearrangement and the diffusion of atoms at the corners that lead to the formation of the curved edges.

Fig. 8b shows a coalescence process at an advanced stage. The particle obviously consists of two grains that may stem from two particles. Fourier transforms were carried out on these two areas and the diffractograms are shown in two different insets. Their lattice fringes have slightly different spacing and orientation and an interface is formed between the two crystallites. Near the interface and the surface of the coalesced particle, a small area with different contrast (within the rectangle in Fig. 8b) can be seen, also showing the rearrangement of atoms.

In addition to the coalescence process documented in Figs. 8a and 8b, overlapping of different phases is also observed. In Fig. 8c the left-upper area and the right-lower area of the image exhibit very different contrasts. The Fourier transform of the right-lower area shows a diffractogram from a single crystallite of Pt<sub>3</sub>Si, while the diffractogram of the left-upper area contains a pair of strong reflections corresponding to the lattice fringes (indicated by the arrow) as well as the reflections arising from Pt (indicated by circles). Therefore, the left-upper area is composed of two phases overlapping with each other. This overlapped crystallite also coalesces with the Pt<sub>3</sub>Si platelet.

## EELS

The energy-loss near edge structure (ELNES) is very sensitive to local coordination of the absorbing atoms and it can give information about electronic structure in bonding. In order to study the silicide formation on the Pt/SiO<sub>2</sub> model system in an independent way, EELS was applied to the as-grown sample and to that after heating in hydrogen at 873 K. On either sample, Si *L* energy-loss spectra were taken from the free silica substrate and from areas covered with Pt particles. After background subtraction and correction for multiple scattering [23], they are plotted in Fig. 9. Before reduction, the Si *L* ELNES from as-grown silica and from the area with Pt particles exhibit the typical Si *L* ELNES of SiO<sub>2</sub>, identical with the one measured from the SiO<sub>2</sub> substrate after treatment as shown in Fig. 9. The onset of the Si *L*<sub>2,3</sub> edge in SiO<sub>2</sub> starts at about 105 eV. The ELNES exhibits two peaks at about 108 and 115 eV respectively, which can be assigned to the excitation of 2p electrons into the 6t<sub>2</sub> and 6a<sub>1</sub> molecule orbits of the SiO<sub>4</sub> tetrahedron [24]. The broad peak at about 131 eV is assigned to an inner-well resonance. The light shoulder at about 107 eV is considered to be due to a bound core exciton [25]. The Si *L*<sub>1</sub> edge is located at about 160 eV.

After the treatment, some new features appear in the Si *L* ELNES spectrum obtained from particle (Fig. 9). The normalized ELNES spectrum from the silica substrate is sub-

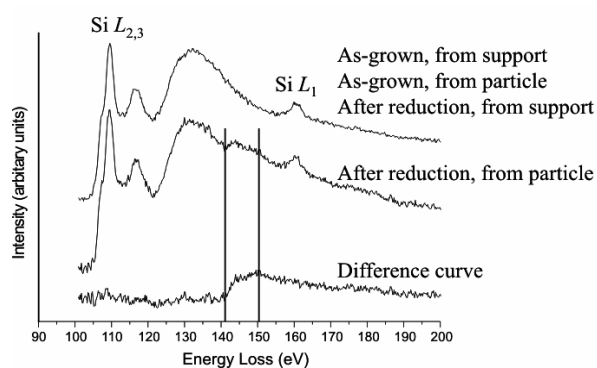


**Fig. 9.** Si L ELNES spectra taken from the free silica substrate and from areas with particles for as-grown sample and that after heating in hydrogen at 873 K. The spectra from the free substrate for the both samples and the spectrum from areas with particles for the as-grown sample exhibit typical SiO<sub>2</sub> features. The spectrum from particle for the reduced sample exhibits new features indicating Si in a changed chemical environment. The difference curve between them is presented.

tracted from it and the difference curve is also shown in Fig. 9. Up to about 140 eV, the ELNES spectrum from particle is similar to that from SiO<sub>2</sub>, indicating the unchanged SiO<sub>4</sub> tetrahedron in the substrate under the supported particles. However, an additional energy loss upon the SiO<sub>2</sub> spectrum is observed, starting from about 141 eV, increasing to the highest point at about 150 eV and gradually decreasing again. This is a signature of silicon in a changed chemical environment compared to SiO<sub>4</sub>, probably due to the formation of silicide, which causes a considerable change in near edge fine structure of Si [26]. Therefore, the EELS also indicates the reduction of silica and the formation of silicide proceeding through the interface between the Pt particle and the silica substrate. To obtain the detailed electronic structure of the silicide, further band structure calculation is necessary.

### Discussion and conclusions

Using electron diffraction, microdiffraction, high-resolution imaging and Fourier transform techniques we could identify platinum silicides of cubic Pt<sub>3</sub>Si with Cu<sub>3</sub>Au structure, monoclinic Pt<sub>3</sub>Si and Pt<sub>12</sub>Si<sub>5</sub> after reducing the Pt/SiO<sub>2</sub> system in hydrogen at 873 K. The formation of silicides was further verified by EELS. The formation of platinum silicides was suggested to result from the reduction of SiO<sub>2</sub> by atomic hydrogen in the presence of platinum [15]. This process involves the dissociative adsorption of hydrogen on platinum particles, the penetration of the metal support interface by atomic hydrogen and the reduction of SiO<sub>2</sub> accompanied by the migration of Si atoms into the Pt particles. In addition, by growing dispersed Pt particles with a common crystalline orientation and regular shapes as the initial state, more information about structural and morphological changes is obtained, which helps to reveal new mechanisms involved in the metal support interaction.

Most particles with platelet shape include unreacted Pt, cubic Pt<sub>3</sub>Si with Cu<sub>3</sub>Au structure and monoclinic Pt<sub>3</sub>Si with distorted Cu<sub>3</sub>Au structure on their simplest zone axes, i.e. the [100] zone axis for Pt and cubic Pt<sub>3</sub>Si, and the [100], [010] or [001] zone axes for monoclinic Pt<sub>3</sub>Si. Moreover, electron diffraction from many particles after the reduction still exhibits spots from Pt<sub>3</sub>Si in the same azimuth orientation as those from Pt. Therefore, a topotactic growth of the Pt<sub>3</sub>Si phase from the Pt particles may take place and this process must involve the migration of Si atoms into the Pt particles. In other systems such as Pt/Al<sub>2</sub>O<sub>3</sub> and Pt/CeO<sub>2</sub>, analogous intermetallic compounds of Pt<sub>3</sub>Me were also observed [21].

The formation of the Pt rich Pt<sub>3</sub>Si phase was assumed as a first step of Pt/SiO<sub>2</sub> interaction under the influence of hydrogen at high temperature [21]. Density functional calculations confirmed the low formation energy and high stability of the initially formed Pt<sub>3</sub>Si. The regular shape of (mostly rectangular platelet-like) Pt<sub>3</sub>Si particles is due to the surface reconstruction under the influence of hydrogen, leading the system to minimum surface energy [27]. Another evidence of the surface reconstruction is that Pt<sub>3</sub>Si (100) planes are observed parallel to the edge in contrast to Pt (100) planes which are rotated by 45° with respect to the edge. The formation of diverging structures with lower Pt content is believed to proceed through the initial Pt<sub>3</sub>Si [21].

However, since the lower Pt content structure does not show any crystallographic coherence with the cubic Pt or Pt<sub>3</sub>Si structure as formulated above and shown in Fig. 1, the mechanism of the mentioned transformation remains unclear. Moreover, our investigation reveals also the coalescence of neighbouring particles and the overlapping of different phases. Curved edges, grain boundaries, truncated corners and other fine structures are observed on the particles containing silicides. Due to all these facts we may conclude that the interaction between Pt and silica, that is usually believed to be a weakly interacting support in comparison with e.g. titania and ceria, is more complicated under the influence of hydrogen at high temperature than it is reported. Thermodynamically, the driving force for the silicide formation is the formation of the stable water molecule, which occurs at the Pt/SiO<sub>2</sub> interface through reaction of the in-diffused atomic hydrogen with the SiO<sub>2</sub> substrate. This interaction may lead to the partial “wetting” of the substrate, flattening of the Pt particles, and migration of Si atoms into the Pt particles. Under the given conditions (flowing system and high temperature), water is easily removed from the system.

Melting and recrystallisation must be taken into account in order to interpret the observed particles of lower Pt content and their morphology (the irregularly shaped Pt<sub>12</sub>Si<sub>5</sub> particles oriented on various zone axes). The reason may be the decreased melting temperature of small particles caused by surface pre-melting and the surface tension of the solid-liquid interface [28], or the reaction enthalpy of the SiO<sub>2</sub> reduction. However, the exothermic nature of the dissociative adsorption of hydrogen on Pt may have little contribu-



tion because hydrogen is admitted at room temperature and then the system is slowly heated to 873 K (within 30 min). The flattening of the particles increases the contacting area with the substrate and the silicide formation also increases the particle size. These effects may cause the as-grown particles with very close spacing to contact with each other and the surface diffusion at high temperature may lead to their coalescence. The overlapping of different phases could be caused either by the migration of crystallites or by the for-

mation of the new phase on the Pt. However, most of the previous investigations on the similar system under similar treatment conditions did not report the migration of particles [6, 18]. More likely, the observed overlapping of phases is due to the formation of the new phase.

### Acknowledgement

This work was in part supported by the Austrian Science Foundation (Project S 8105).

### References

- [1] G.L. Haller, D.E. Resasco, *Adv. Catal.* 36 (1989) 173.
- [2] G.J. den Otter, F.M. Dautzenberg, *J. Catal.* 53 (1978) 116.
- [3] G. Rupprechter, G. Seeber, H. Goller, K. Hayek, *J. Catal.*, 186 (1999) 201.
- [4] C.R. Henry, *Surf. Sci. Rep.* 31 (1998) 235.
- [5] M. Bäumer, H.J. Freund, *Prog. Surf. Sci.* 61 (1999) 127.
- [6] G. Rupprechter, H.J. Freund, *Top. Catal.* 14 (2001) 1.
- [7] G. Rupprechter, K. Hayek, L. Rendón, M. José-Yacamán, *Thin Solid Films* 260 (1995) 148.
- [8] G. Rupprechter, K. Hayek, H. Hofmeister, *J. Catal.* 173 (1998) 409.
- [9] T. Wang, C. Lee, L.D. Schmidt, *Surf. Sci.* 163 (1985) 181.
- [10] P.J.F. Harris, *Surf. Sci.* 185 (1987) L459.
- [11] R. Lamber, N. Jaeger, G. Schulz-Ekloff, *Surf. Sci.* 227 (1990) 268.
- [12] R. Lamber, N. Jaeger, G. Schulz-Ekloff, *J. Catal.* 123 (1990) 285.
- [13] W. Juszczyk, D. Lomot, J. Pielaszek, Z. Karpinski, *Catal. Lett.* 78 (2002) 95.
- [14] R. Lamber, *Thin Solid Films* 128 (1985) L29.
- [15] R. Lamber, N. Jaeger, *J. Appl. Phys.* 70 (1991) 457.
- [16] J. Zhu, G.A. Somorjai, *Nano Lett.* 1 (2001) 8.
- [17] G. Rupprechter, A.S. Eppler, A. Avoyan, G.A. Somorjai, *Stud. Surf. Sci. Catal.* 130 (2000) 215.
- [18] A.S. Eppler, G. Rupprechter, E.A. Anderson, G.A. Somorjai, *J. Phys. Chem. B* 104 (2000) 7286.
- [19] R. Gohle, K. Schubert, *Z. Metallk.* 55 (1964) 503.
- [20] W. Gold, K. Schubert, *Z. Krist.* 128 (1969) 406.
- [21] S. Penner, D. Wang, D.S. Su, G. Rupprechter, R. Podloucky, R. Schlögl, K. Hayek, *Surf. Sci.*, in press.
- [22] P. Stadelmann, *Ultramicroscopy* 21 (1987) 131.
- [23] F.R. Egerton, *Electron Energy-Loss Spectroscopy*. Plenum Press, New York, 1989.
- [24] J.A. Tossell, *J. Am. Chem. Soc.* 97 (1975) 4840.
- [25] P.E. Batson, *Inst. Phys. Conf. Ser. No 117, Section 2* (1991) 55.
- [26] S.J. Naftel, A. Bzowski, T.K. Sham, D.-X. Xu, S.R. Das, *J. Phys. IV* 7 (1997) C2-1131.
- [27] A.-C. Shi and R.I. Masel, *J. Catal.* 120 (1989) 421.
- [28] Z.L. Wang, J.M. Petroski, T.C. Green, M.A. El-Sayed, *Phys. Chem. B* 102 (1998) 6145.